BIOCHEMISTRY
including biophysical chemistry & molecular biology

Article

pubs.acs.org/biochemistry

Molecular Origin of the Binding of WWOX Tumor Suppressor to ErbB4 Receptor Tyrosine Kinase

Brett J. Schuchardt,[†] Vikas Bhat,[†] David C. Mikles,[†] Caleb B. McDonald,[†] Marius Sudol,[‡,§] and Amjad Farooq*[,†]

[†]Department of Biochemistry and Molecular Biology, Leonard Miller School of Medicine, University of Miami, Miami, Florida 33136, United States

[‡]Weis Center for Research, Geisinger Health System, Danville, Pennsylvania 17822, United States

[§]Department of Medicine, Mount Sinai School of Medicine, New York, New York 10029, United States

ABSTRACT: The ability of WWOX tumor suppressor to physically associate with the intracellular domain (ICD) of ErbB4 receptor tyrosine kinase is believed to play a central role in downregulating the transcriptional function of the latter. Herein, using various biophysical methods, we show that while the WW1 domain of WWOX binds to PPXY motifs located within the ICD of ErbB4 in a physiologically relevant manner, the WW2 domain does not. Importantly, while the WW1 domain absolutely requires the integrity of the PPXY consensus sequence, nonconsensus residues within and flanking this motif do not appear to be critical for binding. This strongly suggests that the WW1 domain of WWOX is rather promiscuous toward its cellular partners. We also provide evidence that the lack of binding of the WW2 domain of WWOX to PPXY motifs is due to the replacement of a signature tryptophan, lining the hydrophobic ligand binding groove, with tyrosine (Y85). Consistent with this notion, the Y85W substitution within the WW2 domain exquisitely restores its binding to PPXY motifs in a manner akin to the binding of the WW1 domain of WWOX. Of particular significance is the observation that the WW2 domain augments the binding of the WW1 domain to ErbB4, implying that the former serves as a chaperone within the context of the WW1−WW2 tandem module of WWOX in agreement with our findings reported previously. Altogether, our study sheds new light on the molecular basis of an important WW−ligand interaction involved in mediating a plethora of cellular processes.

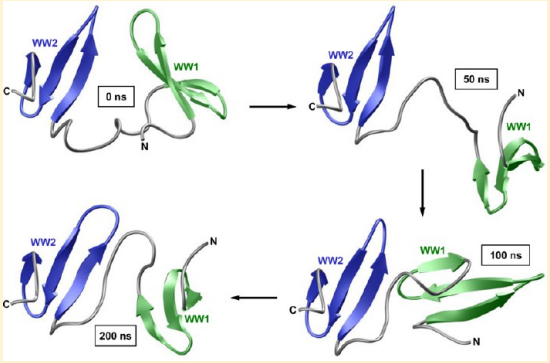

While the role of ErbB4 receptor tyrosine kinase in mediating transmembrane signaling and the fact that the kinase is a prognostic factor in many human diseases are well-documented,[1−8] its complex structural architecture continues to surprise us in terms of its ability to modulate downstream cellular activities via novel modes of action. Notably, ErbB4 harbors the canonical ECD−TM−ICD modular cassette, where the central single-helix transmembrane (TM) domain is between an N-terminal extracellular domain (ECD) and a C-terminal intracellular domain (ICD) (Figure 1a). Upon stimulation with its extracellular ligand heregulin or in response to TPA-induced activation of protein kinase C, ErbB4 undergoes intracellular proteolytic cleavage by γ-secretase.[9,10] This action releases the ICD and marks the initiation of ErbB4 intracellular signaling in what appears to be a relatively new paradigm of signal transduction.[11,12] In particular, similar mechanisms have also been reported for the proteolytic processing of the Notch receptor and the Alzheimer's amyloid precursor protein.[13−15]

Importantly, the ICD of ErbB4 contains putative PPXY motifs (designated PY1−PY3) that serve as recognition sites for the recruitment of WW-containing proteins such as YAP transcriptional regulator,[16,17] WWOX tumor suppressor,[18] and ITCH ubiquitin ligase.[19] The physical association between YAP and ICD facilitates translocation of the latter to the nucleus,[16] where it is believed to regulate the transcription of hitherto unidentified target genes involved in key cellular processes, including embryonic development.[20] It should be noted here that the ICD of ErbB4 is a much more potent co-activator of YAP2 than YAP1.[16] While YAP acts as transcriptional co-activator of ErbB4, interaction with WWOX not only results in cytoplasmic sequestration of the ICD but also suppresses its transcriptional co-activation by YAP.[18] On the other hand, binding to ITCH promotes polyubiquitination and degradation of ErbB4, thereby regulating its stability and the availability of the ICD for subsequent transcriptional regulation in the nucleus.[19] In this manner, WWOX and ITCH antagonize the co-activation function of YAP by virtue of their ability to bind to the ICD of ErbB4 in a competitive manner. In this study, we focus our efforts on uncovering the molecular basis of

Received: July 23, 2013
Revised: December 3, 2013
Published: December 5, 2013

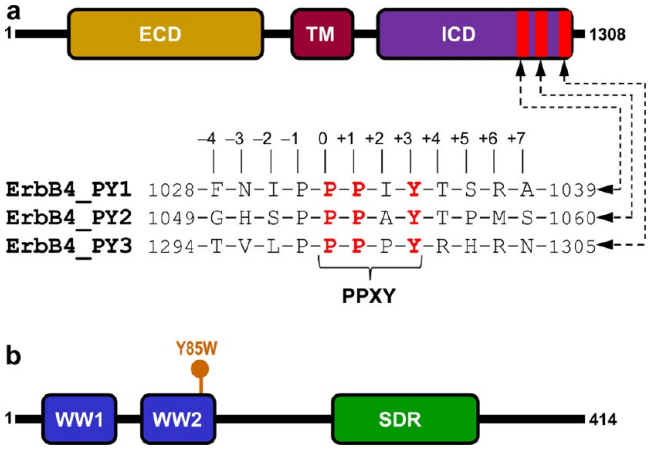

Figure 1. Modular organization of human ErbB4 and WWOX proteins. (a) ErbB4 contains the canonical ECD−TM−ICD receptor tyrosine kinase modular cassette, where the central single-helix transmembrane (TM) domain is between an N-terminal extracellular domain (ECD) and a C-terminal intracellular domain (ICD). The three PPXY motifs (designated PY1−PY3) within the ICD are located at the extreme C-terminus. Note that the amino acid sequence of 12-mer peptides containing the PPXY motifs and flanking residues are provided. The numerals indicate the nomenclature used in this study to distinguish residues within and flanking the motifs relative to the first proline within the PPXY motifs, which is arbitrarily assigned to zero. (b) WWOX is comprised of a tandem copy of WW domains, designated WW1 and WW2, located N-terminal to the short chain dehydrogenase/reductase (SDR) domain. The location of the Y85W mutation within the WW2 domain is indicated.

WWOX−ErbB4 interaction. The fact that WWOX and ErbB4 are co-expressed in breast cancer renders our study all the more relevant and timely.[21]

The WWOX tumor suppressor, comprised of a tandem copy of WW domains (designated WW1 and WW2) located N-terminal to the short chain dehydrogenase/reductase (SDR) domain (Figure 1b), orchestrates a diverse array of cellular activities, including growth, proliferation, apoptosis, and tumor suppression.[22−25] In particular, the WWOX gene spans the 16q23 fragile chromosomal region involved in cancer. The fact that the aberrant expression of WWOX tumor suppressor is believed to be linked to the progression of many forms of cancer, including those of breast and prostate,[26−33] is telling. Moreover, disruption of the WWOX gene in mice results in defective metabolism, impaired growth, and postnatal lethality, implying that WWOX serves a nonredundant role that cannot be compensated by other cellular proteins.[34−36] This argument is further supported by the fact that WWOX is expressed in several distinct isoforms across various tissues, thereby further complicating its role in cellular signaling networks central to health and disease. In addition to its key role in mediating the transcriptional regulation of ErbB4,[18] WWOX also serves as a transcriptional regulator of a diverse array of other ligands such as p73, RUNX, AP2, and NF-κB transcription factors as well as many other cellular proteins, including SIMPLE, Ezrin, and WBP1/2.[22,37−39] Most importantly, the WWOX−ligand interactions are believed to be largely driven by the binding of proline-rich PPXY motifs found within cognate ligands to the WW domains of WWOX in a canonical manner.[40−42]

To understand the molecular basis of WWOX−ErbB4 interaction, we provide herein a detailed analysis of the binding of WW domains of WWOX to PPXY motifs located within the ICD of ErbB4 using various biophysical methods. Our study shows that while the WW1 domain of WWOX binds to PPXY motifs located within the ICD of ErbB4 in a physiologically relevant manner, the WW2 domain does not. This notion thereby further corroborates our previous finding that WW2 likely serves as an orphan domain.[43] We also provide evidence that the lack of binding of the WW2 domain is due to the replacement of a signature tryptophan that forms a part of the network of residues lining the canonical hydrophobic binding groove within the triple-stranded β-sheet fold of WW domains, with tyrosine (Y85). Of particular significance is the observation that the WW2 domain augments the binding of the WW1 domain to ErbB4, implying that the former serves as a chaperone within the context of the WW1−WW2 tandem module of WWOX in agreement with our findings reported previously.[43]

MATERIALS AND METHODS

Protein Preparation. The WW1 domain (residues 16−50), WW2 domain (residues 57−91), and WW1−WW2 tandem module (residues 16−91) of human WWOX were cloned into pET30 bacterial expression vectors with an N-terminal His tag using Novagen LIC technology as described previously.[43] The mutant construct containing the Y85W single substitution within the WW2 domain (WW2W) was generated using the polymerase chain reaction primer extension method.[44] All recombinant proteins were subsequently expressed in the *Escherichia coli* BL21*(DE3) bacterial strain (Invitrogen) and purified on a Ni-NTA affinity column using standard procedures as described previously.[43] Further treatment on a Hiload Superdex 200 size-exclusion chromatography (SEC) column coupled in-line with a GE Akta fast performance liquid chromatography (FPLC) system led to purification of recombinant domains to apparent homogeneity as judged by sodium dodecyl sulfate−polyacrylamide gel electrophoresis analysis. The final yield was typically between 50 and 100 mg of protein of apparent homogeneity per liter of bacterial culture. The protein concentration was determined spectrophotometrically on the basis of extinction coefficients calculated for each recombinant construct using the online software ProtParam at ExPasy Server.[45]

Peptide Synthesis. The 12-mer wild-type and mutant peptides spanning various PPXY motifs within the ICD of human ErbB4 were commercially obtained from GenScript Corp. The amino acid sequence of these peptides is shown in Figure 1a. The peptide concentrations were measured gravimetrically.

Isothermal Titration Calorimetry. Isothermal titration calorimetry (ITC) experiments were performed on a Microcal VP-ITC instrument. All measurements were repeated at least three times. Briefly, WW domains of WWOX alone or in the context of the WW1−WW2 tandem module and ErbB4 peptides were dialyzed in 50 mM sodium phosphate, 100 mM NaCl, 1 mM EDTA, and 5 mM β-mercaptoethanol (pH 7.0). All experiments were initiated by injecting 25 × 10 μL aliquots of each ErbB4 peptide (4 mM) from the syringe into the calorimetric cell containing 1.46 mL of 40−60 μM WW domains of WWOX alone or in the context of the WW1−WW2 tandem module at 25 °C. The change in thermal power as a function of each injection was automatically recorded using the ORIGIN software, and the raw data were further processed to yield binding isotherms of heat release per injection as a function of the molar ratio of each peptide to the WW domain

dx.doi.org/10.1021/bi400987k | *Biochemistry* 2013, 52, 9223−9236

construct. The heats of mixing and dilution were subtracted from the heat of binding per injection by conducting a control experiment in which the same buffer in the calorimetric cell was titrated against each peptide in an identical manner. To extract the equilibrium dissociation constant (K_d) and the enthalpic change (ΔH) associated with binding, the ITC isotherms were iteratively fit to a one-site binding model by nonlinear least-squares regression analysis using the integrated ORIGIN software as described previously.[43,46] Notably, all binding stoichiometries were fixed to unity, while ΔH and K_d were allowed to float during the fitting procedure to improve the accuracy of the thermodynamic parameters. The free energy change (ΔG) upon peptide binding was calculated from the relationship

$$\Delta G = RT \ln K_d \quad (1)$$

where R is the universal molar gas constant (1.99 cal K^{-1} mol^{-1}) and T is the absolute temperature. The entropic contribution ($T\Delta S$) to the free energy of binding was calculated from the relationship

$$T\Delta S = \Delta H - \Delta G \quad (2)$$

where ΔH and ΔG are as defined above.

Analytical Light Scattering. Analytical light scattering (ALS) experiments were conducted at 10 °C on a Wyatt miniDAWN TREOS triple-angle static light scattering detector and Wyatt QELS dynamic light scattering detector coupled in-line with a Wyatt Optilab rEX differential refractive index detector and interfaced with a Hiload Superdex 200 size-exclusion chromatography (SEC) column under the control of a GE Akta FPLC system. Briefly, WW domains of WWOX alone or in the context of the WW1−WW2 tandem module were dialyzed in 50 mM sodium phosphate, 100 mM NaCl, 1 mM EDTA, and 5 mM β-mercaptoethanol (pH 7.0). Each protein construct was loaded onto the SEC column at a starting concentration of 100−200 μM and at a flow rate of 1 mL/min, and data were automatically acquired using the ASTRA software. The angular and concentration dependence of the static light scattering (SLS) intensity of each protein construct resolved in the flow mode were measured with the Wyatt miniDAWN TREOS detector. The SLS data were analyzed according to the following built-in Zimm equation in the ASTRA software:[47,48]

$$(Kc)/R_\theta = (1/M + 2A_2c)\{1 + [16\pi^2(R_g)^2/3\lambda^2] \sin^2(\theta/2)\} \quad (3)$$

where R_θ is the excess Raleigh ratio due to protein in solution as a function of protein concentration c (milligrams per milliliter) and the scattering angle θ (42°, 90°, and 138°), M is the observed molar mass of each protein species, A_2 is the second virial coefficient, λ is the wavelength of laser light in solution (658 nm), R_g is the radius of gyration of the protein, and K is given by the following relationship:

$$K = [4\pi^2 n^2 (dn/dc)^2]/(N_A\lambda^4) \quad (4)$$

where n is the refractive index of the solvent, dn/dc is the refractive index increment of the protein in solution, and N_A is Avogadro's number (6.02×10^{23} mol^{-1}). At dilute protein concentrations ($c \rightarrow 0$), eq 3 reduces to

$$(Kc)/R_\theta = 1/M + [16\pi^2(R_g)^2/(3M\lambda^2)] \sin^2(\theta/2) \quad (5)$$

Thus, a plot of $(Kc)/R_\theta$ versus $\sin^2(\theta/2)$ yields a straight line with a slope of $(16\pi^2R_g^2)/(3M\lambda^2)$ and a y-intercept of $1/M$. It should be noted here that the light scattered by the WW domains of WWOX alone or in the context of the WW1−WW2 tandem module displayed no observable angular dependence, thereby rendering the determination of R_g for each construct unpractical. Nonetheless, M was obtained in a global analysis from the y-intercept of linear fits of a series of $(Kc)/R_\theta$ − $\sin^2(\theta/2)$ plots as a function of protein concentration along the elution profile of each protein species using SLS measurements at three scattering angles. The weighted-average molar mass (M_w) and number-average molar mass (M_n) were calculated from the following relationships:

$$M_w = \sum(c_iM_i)/\sum c_i \quad (6)$$

$$M_n = \sum c_i/\sum(c_i/M_i) \quad (7)$$

where c_i is the protein concentration and M_i is the observed molar mass at the ith slice within an elution profile. The time and concentration dependence of dynamic light scattering (DLS) intensity fluctuation of each protein construct resolved in the flow mode were measured by the Wyatt QELS detector positioned at 90° with respect to the incident laser beam. The DLS data were iteratively fit using nonlinear least-squares regression analysis to the following built-in equation in the ASTRA software:[49−51]

$$G(\lambda) = \alpha \exp(-2\Gamma\tau) + \beta \quad (8)$$

where $G(\tau)$ is the autocorrelation function of dynamic light scattering intensity fluctuation I, τ is the delay time of the autocorrelation function, Γ is the decay rate constant of the autocorrelation function, α is the initial amplitude of the autocorrelation function at zero delay time, and β is the baseline offset (the value of the autocorrelation function at an infinite delay time). Thus, fitting the equation given above to a range of $G(\tau)-\tau$ plots as a function of protein concentration along the elution profile of each protein species was used to compute the weighted-average value of Γ using DLS measurements at a scattering angle of 90°. Next, the translational diffusion coefficient (D_t) of each protein species was calculated from the following relationship:

$$D_t = (\Gamma\lambda^2)/[16\pi^2n^2 \sin^2(\theta/2)] \quad (9)$$

where λ is the wavelength of laser light in solution (658 nm), n is the refractive index of the solvent, and θ is the scattering angle (90°). Additionally, the hydrodynamic radius (R_h) of each protein construct was determined from the Stokes−Einstein relationship:

$$R_h = (k_BT)/(6\pi\eta D_t) \quad (10)$$

where k_B is Boltzman's constant (1.38×10^{-23} J K^{-1}), T is the absolute temperature, and η is the solvent viscosity. Notably, the R_h reported here represents the weighted-average value as defined by the following expression:

$$R_h = \sum(c_iR_{h,i})/\sum c_i \quad (11)$$

where c_i is the protein concentration and $R_{h,i}$ is the observed hydrodynamic radius at the ith slice within an elution profile. It is also noteworthy that, in both the SLS and DLS measurements, the protein concentration (c) along the elution profile of each protein species was automatically quantified in the ASTRA

dx.doi.org/10.1021/bi400987k | Biochemistry 2013, 52, 9223−9236

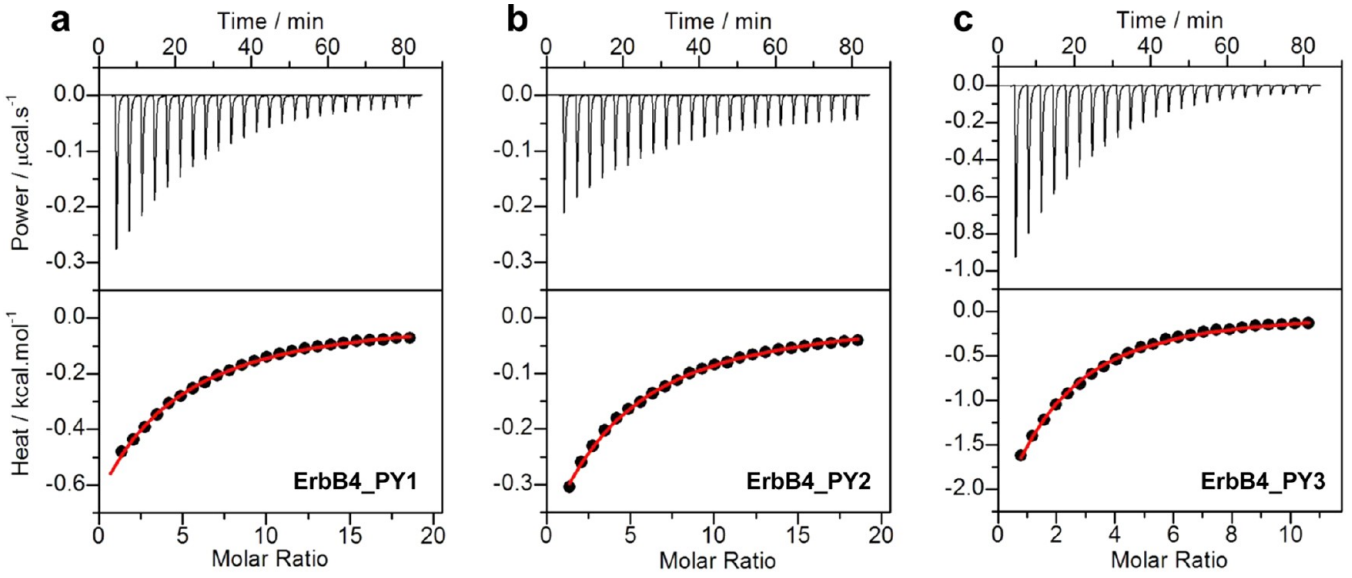

Figure 2. ITC analysis for the binding of the WW1 domain of WWOX to ErbB4_PY1 (a), ErbB4_PY2 (b), and ErbB4_PY3 (c) peptides. The top panels show the raw ITC data expressed as the change in thermal power with respect to time over the period of titration. In the bottom panels, the change in molar heat is expressed as a function of the molar ratio of the corresponding peptide to the WW1 domain. The red lines in the bottom panels show the fit of data to a one-site binding model using the integrated ORIGIN software as described previously.[43,46]

Table 1. Thermodynamic Parameters for the Binding of the WW1 Domain of WWOX to PPXY Peptides Derived from the ICD of ErbB4[a]

Peptide	Sequence	K_d / µM	ΔH / kcal.mol^{-1}	TΔS / kcal.mol^{-1}	ΔG / kcal.mol^{-1}
ErbB4_PY1	FNIP**PP**I**Y**TSRA	383 ± 30	-6.88 ± 0.48	-2.21 ± 0.43	-4.67 ± 0.05
ErbB4_PY2	GHSP**PP**A**Y**TPMS	362 ± 45	-3.66 ± 0.33	+1.04 ± 0.40	-4.70 ± 0.07
ErbB4_PY3	TVLP**PP**P**Y**RHRN	144 ± 16	-6.21 ± 0.54	-1.24 ± 0.10	-5.25 ± 0.06

[a]All parameters were obtained from ITC measurements at pH 7.0 and 25 °C. Note that the consensus residues within the PPXY motif of each peptide are colored blue for the sake of clarity. All binding stoichiometries were fixed to unity. Errors were calculated from at least three independent measurements. All errors are given to one standard deviation.

software from the change in the refractive index (Δn) with respect to the solvent as measured by the Wyatt Optilab rEX detector using the following relationship:

$$c = (\Delta n)/(dn/dc) \quad (12)$$

where dn/dc is the refractive index increment of the protein in solution.

Molecular Modeling. Molecular modeling (MM) was employed to build atomic structures of WW1 and WW2 domains of WWOX in the context of a tandem module and individually in complex with a peptide containing the PY3 motif located within the ICD of ErbB4 (ErbB4_PY3) using the MODELER software based on homology modeling.[52] For individual liganded WW domains, the NMR structure of the homologous WW domain of YAP bound to a peptide containing the PPXY motif was used as a template [Protein Data Bank (PDB) entry 1JMQ]. For the unliganded tandem WW1−WW2 module, the NMR structure of the tandem WW1−WW2 module of FBP21 was used as a template (PDB entry 2JXW). A total of 100 atomic models were calculated, and the structure with the lowest energy, as judged by the MODELER Objective Function, was selected for further analysis. The atomic models were rendered using RIBBONS.[53]

Molecular Dynamics. Molecular dynamics (MD) simulations were performed with GROMACS[54] using the integrated AMBER99SB-ILDN force field.[55] Briefly, the structural models of WW1 and WW2 domains of WWOX in the context of a tandem module and individually in complex with the ErbB4_PY3 peptide were each centered in a cubic box with dimensions of 10 Å and hydrated using the extended simple point charge (SPC/E) water model.[56] The ionic strength of the solution was set to 100 mM with NaCl, and the hydrated structures were energy-minimized with the steepest descent algorithm prior to equilibration under the *NPT* ensemble conditions, wherein the number of atoms (N), pressure (P), and temperature (T) within the system were kept constant. The particle mesh Ewald (PME) method[57] was employed to compute long-range electrostatic interactions with a spherical cutoff of 10 Å and a grid space of 1.6 Å with a fourth-order interpolation. The Linear Constraint Solver (LINCS) algorithm was used to restrain bond lengths.[58] All MD simulations were performed under periodic boundary conditions (PBC) at 300 K

Table 2. Thermodynamic Parameters for the Binding of the WW1 Domain of WWOX to the Wild Type (PY3_WT) and Single-Alanine Mutants of the ErbB4_PY3 Peptide[a]

Peptide	Sequence	K_d / μM	ΔH / kcal.mol^{-1}	TΔS / kcal.mol^{-1}	ΔG / kcal.mol^{-1}
PY3_WT	TVLPPPPYRHRN	144 ± 16	-6.21 ± 0.54	-1.24 ± 0.10	-5.25 ± 0.06
PY3_A-3	TALPPPPYRHRN	113 ± 21	-3.67 ± 0.23	+1.73 ± 0.34	-5.40 ± 0.11
PY3_A-2	TVAPPPPYRHRN	151 ± 15	-6.19 ± 0.60	-1.32 ± 1.16	-5.22 ± 0.07
PY3_A-1	TVLAPPPYRHRN	161 ± 29	-3.33 ± 0.42	+1.86 ± 0.52	-5.19 ± 0.11
PY3_A0	TVLPAPPYRHRN	NBD	NBD	NBD	NBD
PY3_A+1	TVLPPAPYRHRN	NBD	NBD	NBD	NBD
PY3_A+2	TVLPPPAYRHRN	287 ± 37	-3.63 ± 0.30	+1.21 ± 0.37	-4.84 ± 0.08
PY3_A+3	TVLPPPPARHRN	NBD	NBD	NBD	NBD
PY3_A+4	TVLPPPPYAHRN	275 ± 64	-4.02 ± 0.24	+0.85 ± 0.38	-4.87 ± 0.14
PY3_A+5	TVLPPPPYRARN	157 ± 18	-11.40 ± 1.41	-6.20 ± 1.48	-5.20 ± 0.07
PY3_A+6	TVLPPPPYRHAN	135 ± 30	-4.78 ± 0.26	+0.52 ± 0.39	-5.29 ± 0.13

[a]All parameters were obtained from ITC measurements at pH 7.0 and 25 °C. Note that the alanine substitutions within the ErbB4_PY3 peptide are colored red and underlined, while the consensus residues within the PPXY motif are colored blue for the sake of clarity. All binding stoichiometries were fixed to unity. Errors were calculated from at least three independent measurements. All errors are given to one standard deviation. NBD indicates no binding determined because of weak interactions (K_d > 1 mM).

using the leapfrog integrator with a time step of 2 fs. For the final MD production runs, data were collected every nanosecond over a time scale of 250 ns. Structural snapshots taken at various intervals during the course of MD simulations were rendered using RIBBONS.[53]

RESULTS AND DISCUSSION

The WW1 Domain of WWOX Binds to PPXY Motifs in ErbB4 with Distinct Affinities. To uncover the molecular basis of WWOX−ErbB4 interaction, we measured the binding of WW domains of WWOX to PPXY peptides derived from potential WWOX binding sites in ErbB4 using ITC. While representative ITC isotherms for the binding of the WW1 domain are shown in Figure 2, no binding of the WW2 domain to any of the PPXY motif was observed, even when external conditions, including temperature, ionic strength, and pH, were altered. This salient observation strongly suggests that the WW2 domain of WWOX does not harbor intrinsic potential to interact with PPXY motifs derived from ErbB4, thereby further corroborating our previous finding that WW2 likely serves as an orphan domain.[43] On the other hand, the WW1 domain binds to all three PPXY motifs located within ErbB4 but in a distinct manner (Table 1). Thus, while binding of the WW1 domain to the ErbB4_PY3 motif occurs with an affinity of slightly greater than 100 μM, it recognizes the ErbB4_PY1 and ErbB4_PY2 motifs on the order of hundreds of micromolar. Despite these differences, binding of the WW1 domain of WWOX to all three PPXY motifs is predominantly driven by favorable enthalpic forces accompanied by small unfavorable or favorable entropic changes. Notably, the enthalpically driven nature of the WW−PPXY interaction suggests the formation of specific intermolecular interactions such as hydrogen bonding and van der Waals contacts that likely underscore the fidelity of this key protein−protein interaction. In contrast, the overall unfavorable entropic changes most likely result from the loss of degrees of freedom available to both partners upon intermolecular association.

To understand the molecular factors that drive the binding of the WW1 domain of WWOX to various PPXY motifs in ErbB4 with differential affinities (Table 1), we next performed an alanine scan on the ErbB4_PY3 peptide and measured the binding of each mutant peptide to the WW1 domain as described above (Table 2). Strikingly, our data reveal that alanine substitution of nonconsensus residues within and flanking the PPXY motif within the ErbB4_PY3 peptide has little effect or a negligible effect on the binding of the WW1 domain. This finding suggests that nonconsensus residues within and flanking the PPXY motifs are not critical for driving the WWOX−ErbB4 interaction but may be important for stabilizing the conformation of PPXY peptides. It is, however, noteworthy that the alanine substitution of residues P+2 and R+4, according to the nomenclature presented in Figure 1a,

dx.doi.org/10.1021/bi400987k | Biochemistry 2013, 52, 9223−9236

within the ErbB4_PY3 peptide slightly mitigates the binding of the WW1 domain. This implies that the presence of a proline and a charged, bulky residue at positions 2 and 4, respectively, may account for the binding of the ErbB4_PY3 peptide to the WW1 domain with an affinity higher than those for the other two peptides. Indeed, residues P+2 and R+4 within the ErbB4_PY3 peptide are replaced with non-proline and noncharged, nonbulky residues, respectively, at the structurally equivalent positions in ErbB4_PY1 and ErbB4_PY2 peptides. In particular, the importance of a proline at the +2 position may be ascribed to its ability to buttress the polyproline II (PPII) helical conformation of the ErbB4_PY3 peptide required for its optimal binding to the WW1 domain.[59−62] Taken together, our thermodynamic analysis shows that the WW1 domain of WWOX binds to ErbB4 peptides in a rather promiscuous fashion with a subtle contribution of nonconsensus residues within and flanking the PPXY motifs to the overall free energy of binding.

Structural Analysis Provides a Physical Basis for the Binding of the WW1 Domain and a Lack Thereof of the WW2 Domain of WWOX to PPXY Motifs within ErbB4. To understand the physical basis of the binding of the WW1 domain and the lack thereof of the WW2 domain of WWOX to PPXY motifs within ErbB4, we built their respective structural models in complex with the ErbB4_PY3 peptide (Figure 3). Our structural analysis reveals that the ErbB4_PY3 peptide adopts the PPII helical conformation and binds within the hydrophobic groove of the triple-stranded β-sheet fold of the WW1 domain in a canonical manner[59−62] (Figure 3a). Consistent with our thermodynamic data presented above (Tables 1 and 2), the consensus residues within the PPXY motif appear to be exclusively engaged in key intermolecular contacts with specific residues lining the hydrophobic groove of the WW1 domain, while nonconsensus residues within and flanking the PPXY motif make no discernible intermolecular contacts. Briefly, the pyrrolidine moiety of P0, the first proline within the PPXY motif according to the nomenclature presented in Figure 1a, stacks against the indole side chain of W44 in the WW1 domain (Figure 3a). It should be noted here that W44 represents one of the two signature tryptophan residues that lend their name to WW domains. On the other hand, the side chain moieties of residues Y33 and T42 within the WW1 domain sandwich the pyrrolidine ring of P+1 within the PPXY motif. Finally, the phenyl moiety of Y+3, the terminal tyrosine within the PPXY motif, is buried deep into the hydrophobic groove and is escorted by side chain atoms of the A35/H37/E40 triad in the WW1 domain.

It is telling that the various interactions between specific side chain groups in the WW1 domain and the ErbB4_PY3 peptide are stabilized by an extensive network of van der Waals contacts and hydrogen bonding (Figure 3a). Importantly, the Hη phenolic hydrogen of the Y+3 residue appears to hydrogen bond with the imidazole Nδ1 atom of H37 in the WW1 domain. On the other hand, the E40 residue in the WW1 domain stabilizes the aromatic ring of Y+3 within the ErbB4_PY3 peptide by virtue of the apolar character of its -CγH2- methylene atoms, while its negatively charged carboxyl group points away to prevent unfavorable contact with Y+3. Of particular note is the observation that the pyrrolidine ring of P+2 within the ErbB4_PY3 peptide in complex with the WW1 domain is fully solvent-exposed (not shown). This strongly suggests that the P+2 residue, which is replaced by a non-proline in ErbB4_PY1 and ErbB4_PY2 peptides, may play an important role in the stabilization of the PPII helical conformation of the ErbB4_PY3 peptide. Accordingly, the presence of a proline at position +2 could account for the binding of the ErbB4_PY3 peptide to the WW1 domain having an affinity higher than those of the other two peptides, as suggested by our thermodynamic data (Tables 1 and 2), by virtue of its ability to lower the entropic penalty to the overall free energy of binding.

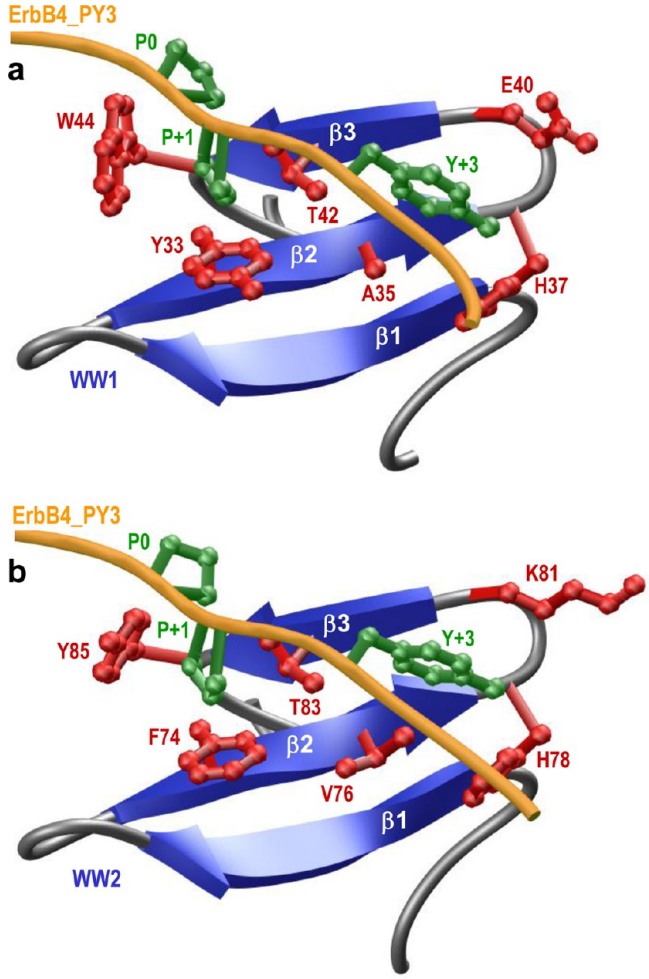

Figure 3. Structural models of WW1 (a) and WW2 (b) domains of WWOX in complex with the ErbB4_PY3 peptide containing the PPXY motif. In each case, the β-strands within the WW domain are colored blue with loops colored gray and the PPXY peptide colored yellow. The side chain moieties of residues within the WW domain and the PPXY peptide engaged in key intermolecular contacts are colored red and green, respectively. Note that the first two N-terminal proline residues within the PPXY motif are P0 and P+1, while the C-terminal Y is denoted as Y+3.

Equally importantly, while our alanine scan suggests that none of the residues flanking the PPXY motif are critical for binding to the WW1 domain in terms of the change in the overall free energy (ΔG), the underlying changes in the enthalpic contribution (ΔH) nonetheless paint a very different picture (Table 2). In particular, the enthalpic change associated with the binding of the mutant PY3_A+5 peptide, harboring an alanine in place of H+5, is concomitant with the release of more than −5 kcal/mol of favorable enthalpy relative to the PY3_WT peptide. While we note the difficulties associated with the accurate determination of ΔH associated with weak macromolecular interactions, it is nevertheless conceivable

dx.doi.org/10.1021/bi400987k | *Biochemistry* 2013, 52, 9223−9236

Table 3. Thermodynamic Parameters for the Binding of the WW2W Domain of WWOX to PPXY Peptides Derived from the ICD of ErbB4[a]

Peptide	Sequence	K_d / μM	ΔH / kcal.mol^{-1}	TΔS / kcal.mol^{-1}	ΔG / kcal.mol^{-1}
ErbB4_PY1	FNIPPPIYTSRA	680 ± 121	-4.74 ± 0.52	-0.40 ± 0.62	-4.33 ± 0.11
ErbB4_PY2	GHSPPPAYTPMS	620 ± 55	-8.08 ± 1.09	-3.70 ± 1.14	-4.38 ± 0.05
ErbB4_PY3	TVLPPPPYRHRN	54 ± 9	-4.15 ± 0.28	+1.68 ± 0.37	-5.83 ± 0.09

[a]All parameters were obtained from ITC measurements at pH 7.0 and 25 °C. Note that the WW2W domain is the mutant construct of the WW2 domain harboring the Y85W substitution. The consensus residues within the PPXY motif of each peptide are colored blue for the sake of clarity. All binding stoichiometries were fixed to unity. Errors were calculated from at least three independent measurements. All errors are given to one standard deviation. NBD indicates no binding determined because of weak interactions (K_d > 1 mM).

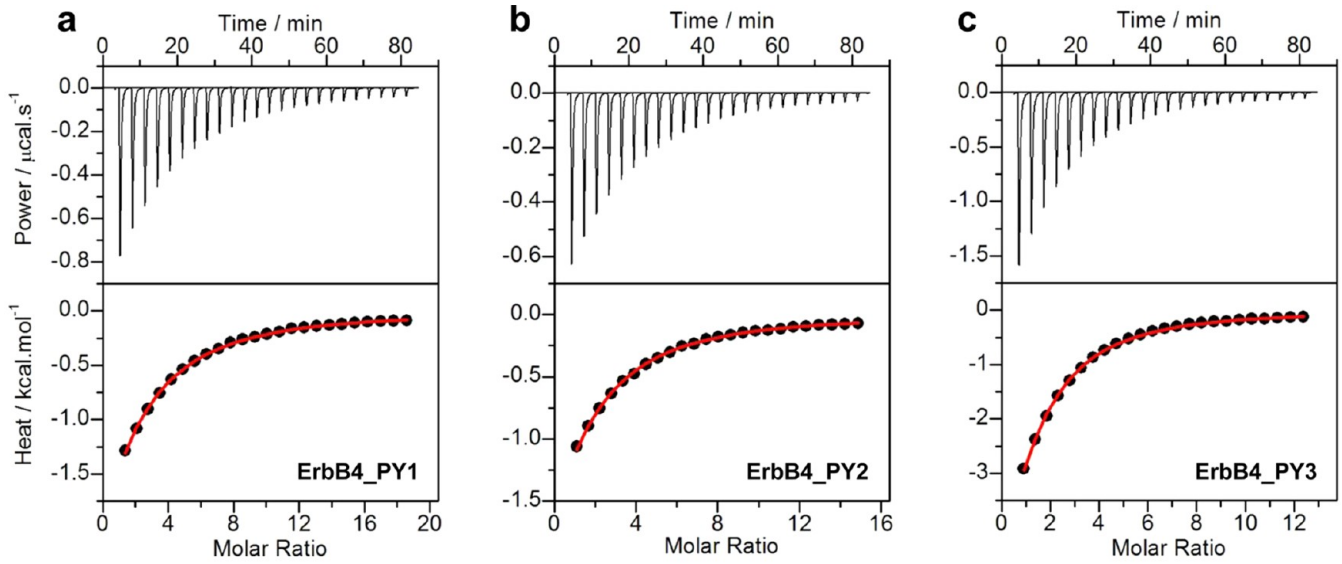

Figure 4. ITC analysis of the binding of the WW1−WW2 tandem module of WWOX to ErbB4_PY1 (a), ErbB4_PY2 (b), and ErbB4_PY3 (c) peptides. The top panels show the raw ITC data expressed as the change in thermal power with respect to time over the period of titration. In the bottom panels, the change in molar heat is expressed as a function of the molar ratio of the corresponding peptide to the WW1−WW2 tandem module. The red lines in the bottom panels show the fit of the data to a one-site binding model using the integrated ORIGIN software as described previously.[43,46]

that the much smaller size of alanine allows the PY3_A+5 mutant peptide to engage in closer intermolecular contacts with the WW1 domain relative to the PY3_WT peptide. However, the resulting release of more favorable enthalpy appears to be offset and largely compensated by an equal but unfavorable change in entropy in agreement with the ubiquitous enthalpy−entropy compensation phenomenon that governs macromolecular interactions (Table 2). It is also noteworthy that water-mediated hydrogen bonding has been recently shown to play a key role in driving the binding of proline-rich ligands to SH3 domains.[63−65] Thus, although the role of water in mediating WW−ligand interactions has not been directly probed, it is possible that hydration also plays an important role in fine-tuning the affinity of various ErbB4 peptides for the WW1 domain of WWOX in addition to the role of specific intermolecular interactions.

More importantly, our structural analysis provides a tantalizing rationale for the lack of binding of the WW2 domain of WWOX to ErbB4 peptides (Figure 3b). The fact that all residues but W44 in the WW1 domain involved in intermolecular contacts with the ErbB4_PY3 peptide are highly conserved within the hydrophobic groove of the WW2 domain is striking. Thus, the Y33/T42 pair in the WW1 domain that serves as a counterpart for accommodating P+1 is substituted by a relatively conservative F74/T83 pair in the WW2 domain. In a similar manner, the A35/H37/E40 triad in the WW1 domain that escorts Y+3 is replaced by a relatively conserved V76/H78/K81 triad in the WW2 domain. However, residue W44 in the WW1 domain, whose indole side chain is involved in the stabilization of P0, is replaced by Y85 in the WW2 domain. Given the distinguishing chemistry and apolar character of the aromatic rings of W44 and Y85, we reason that this tyrosine for tryptophan substitution within the WW2 domain most likely accounts for its lack of binding to PPXY motifs. To test the validity of this hypothesis, we introduced the Y85W substitution within the WW2 domain and subsequently measured the binding of this mutant WW2 domain, hereafter termed the WW2W domain, to various ErbB4 peptides using ITC (Table 3). Our data indicate that while the WW2W mutant domain recognizes ErbB4_PY1 and ErbB4_PY2

dx.doi.org/10.1021/bi400987k | *Biochemistry* 2013, 52, 9223−9236

Table 4. Thermodynamic Parameters for the Binding of the WW1−WW2 Tandem Module of WWOX to PPXY Peptides Derived from the ICD of ErbB4[a]

Peptide	Sequence	K_d / μM	ΔH / kcal.mol^{-1}	TΔS / kcal.mol^{-1}	ΔG / kcal.mol^{-1}
ErbB4_PY1	FNIP**PP**I**Y**TSRA	170 ± 12	-7.25 ± 0.88	-2.10 ± 0.92	-5.15 ± 0.04
ErbB4_PY2	GHSP**PP**A**Y**TPMS	175 ± 13	-4.88 ± 0.28	+0.26 ± 0.34	-5.13 ± 0.05
ErbB4_PY3	TVLP**PP**P**Y**RHRN	68 ± 8	-5.00 ± 0.30	+0.70 ± 0.37	-5.70 ± 0.07

[a]All parameters were obtained from ITC measurements at pH 7.0 and 25 °C. Note that the consensus residues within the PPXY motif of each peptide are colored blue for the sake of clarity. All binding stoichiometries were fixed to unity. Errors were calculated from at least three independent measurements. All errors are given to one standard deviation.

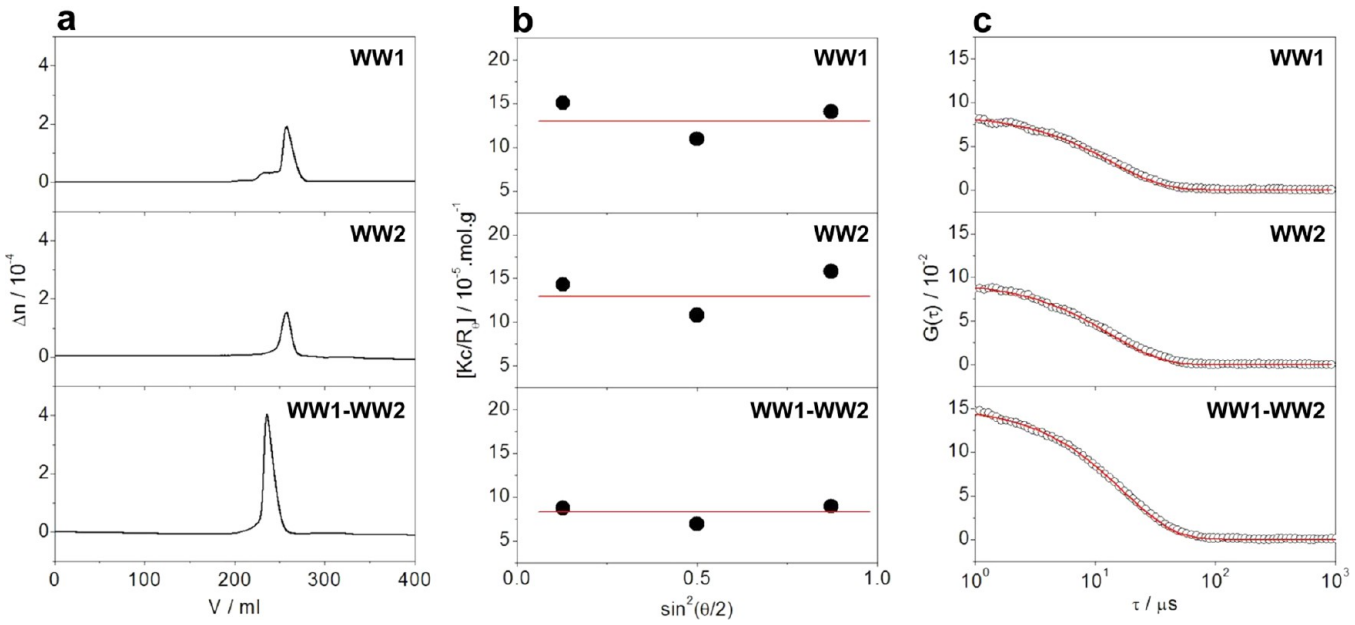

Figure 5. ALS analysis of WW1 (top) and WW2 (middle) domains alone and in the context of the WW1−WW2 tandem module (bottom) of WWOX. (a) Elution profiles as monitored by the differential refractive index (Δn) of each protein construct plotted as a function of elution volume (V). (b) Partial Zimm plots obtained for each protein construct from analytical SLS measurements. Note that the red lines through the data points represent linear fits. (c) Autocorrelation function plots obtained for each protein construct from analytical DLS measurements. Note that the red lines represent nonlinear least-squares fits of the data to an autocorrelation function as embodied in eq 8.

peptides rather weakly, it binds to the ErbB4_PY3 peptide with an affinity that is more than 2-fold stronger than that observed for the binding of the WW1 domain (Tables 1 and 3). Taken together, these findings have an important implication for the engineering of WW domains of WWOX for therapeutic intervention.

The WW2 Domain Augments the Binding of the WW1 Domain in the Context of the WW1−WW2 Tandem Module of WWOX to PPXY Motifs within ErbB4. We previously reported that while the WW1 domain of WWOX is structurally disordered and folds upon ligand binding,[43] the WW2 domain not only adopts a fully structured conformation but also aids in the stabilization and binding of the ligand to the WW1 domain. On the basis of this earlier finding, we postulate that the WW2 domain likely serves as a chaperone to augment the physiological function of the WW1 domain within WWOX. To test this hypothesis further, we next conducted ITC analysis on the binding of the WW1−WW2 tandem module of WWOX to various ErbB4 peptides (Figure 4). Conspicuously, our data show that the WW1 domain in the context of the WW1−WW2 tandem module binds to ErbB4 peptides with affinities that are more than 2-fold stronger than those observed for the binding of the WW1 domain alone (Tables 1 and 4).

WW Domains May Lie Close to Each Other within the WW1−WW2 Tandem Module of WWOX. The data presented above, and those reported previously,[43] strongly establish the role of the WW2 domain of WWOX as a chaperone in its ability to modulate binding of the ligand to the WW1 domain. The physical basis of how the WW2 domain mediates such an allosteric effect, however, warrants further investigation. Thus, for example, it is conceivable that the WW2 domain physically associates with the WW1 domain and, in so doing, aids its folding. This notion gains further credibility in light of the rather short linker (fewer than 20 residues) separating the tandem WW domains. On the other hand, it is also conceivable that the WW1−WW2 tandem module adopts a colinear "dumbbell-like" conformation. Finally, the possibility that the WW1−WW2 tandem module self-associates into a

dx.doi.org/10.1021/bi400987k | *Biochemistry* 2013, 52, 9223−9236

Table 5. Hydrodynamic Parameters for WW Domains Alone and in the Context of the WW1−WW2 Tandem Module of WWOX[a]

construct	M_w (kDa)	M_n (kDa)	M_w/M_n	R_h (Å)	associativity
WW1	9 ± 2	9 ± 1	1.06 ± 0.08	18 ± 1	monomer
WW2	10 ± 1	9 ± 1	1.02 ± 0.03	19 ± 1	monomer
WW1−WW2	14 ± 1	14 ± 1	1.03 ± 0.04	27 ± 1	monomer

[a]All parameters were obtained from ALS measurements at pH 7.0 and 25 °C. Note that the calculated molar masses of recombinant WW1, WW2, and WW1−WW2 constructs from their respective amino acid sequence are 9, 9, and 14 kDa, respectively. Errors were calculated from at least three independent measurements. All errors are given to one standard deviation.

dimer or a higher-order oligomer to adopt quaternary structure cannot be ruled out either. This latter view is supported by the observation that the WW2 domain of the SAV1 adaptor, which shares a high degree of sequence homology with the WW2 domain of WWOX and has no known ligand, self-associates into a homodimer.[66]

In an effort to shed light on the physical basis of how the WW2 domain modulates binding of the ligand to the WW1 domain, we next performed ALS analysis on WW domains of WWOX alone and in the context of the WW1−WW2 tandem module (Figure 5). Importantly, we also quantified various physical parameters accompanying the solution behavior of WW domains from the first principles of hydrodynamics without any assumptions (Table 5). Our data indicate that WW domains alone and in the context of the WW1−WW2 tandem module predominantly adopt a monomeric conformation in solution. This is evidenced by the fact that the observed molar mass for all species in solution is in remarkable agreement with their corresponding molar mass calculated from their amino acid sequence alone (Table 5). Notably, the WW1 domain also harbors some propensity to homodimerize, as indicated by a small left-hand shoulder in the corresponding elution profile (Figure 5a). However, the homodimer−monomer equilibrium appears to be largely in favor of the latter species. Given that the ALS analysis was conducted at high protein concentrations (100−200 μM), a practical necessity because of the rather low sensitivity of light scattering detectors, we believe that the propensity of the WW1 domain to homodimerize is unlikely to be physiologically relevant. Most importantly, the lack of angular dependence of static light scattering is indicative of the fact that WW domains alone or in the context of the WW1−WW2 tandem module do not self-associate into higher-order oligomers (Figure 5b). This notion is further vindicated by the fact that the M_w/M_n ratio is close to unity for all species (Table 5), implying that the WW domains alone and in the context of the WW1−WW2 tandem module are highly monodisperse.

To gain insights into macromolecular conformation, we also calculated the hydrodynamic radius (R_h) for each species on the basis of dynamic light scattering (Figure 5c and Table 5). Such analysis reveals that while both WW domains alone display a hydrodynamic radius of ∼20 Å, it only slightly increases in the case of the WW1−WW2 tandem module. While this is indicative of the fact that the WW domains may lie close to the WW1−WW2 tandem module, the alternative possibility that they may also physically associate with each other cannot be excluded either. To test this plausible scenario, we conducted ITC analysis on the binding of the WW1 domain of WWOX to the WW2 domain and vice versa. Interestingly, our analysis revealed no observable binding between the two WW domains. However, this does not necessarily preclude their physical association in the context of a tandem module, wherein they are physically connected by a short linker. For example, the presence of an interdomain linker is likely to significantly lower the entropic penalty associated with their physical association.

The WW1−WW2 Tandem Module of WWOX Displays Dynamic Plasticity. To further test the extent to which WW domains of WWOX may physically associate with each other, we next conducted MD simulations on the WW1−WW2 tandem module (Figure 6). Briefly, the starting MD conformation of the WW1−WW2 tandem module of WWOX was structurally modeled on the basis of its homology with the tandem WW1−WW2 module of FBP21 pre-mRNA splicing factor.[67] As shown in Figure 6a, the MD trajectory reveals that the WW1−WW2 tandem module undergoes a rapid "burst" phase over the first 50 ns and then slowly reaches structural equilibrium with a root-mean-square deviation (rmsd) for the backbone atoms in the neighborhood of 10 Å. This rather large rmsd value is strongly indicative of the fact that the WW domains are unlikely to be physically associated with each other and most probably experience large degrees of freedom relative to each other.

To further glean insights into the origin of such relative flexibility, we also analyzed the root-mean-square fluctuation (rmsf) of backbone atoms over the course of the MD simulation (Figure 6b). Remarkably, our rmsf analysis reveals that the overall lack of stability of the WW1−WW2 tandem module arises from the rather large fluctuations within each of the two constituent WW domains in lieu of the interdomain linker. Notably, the WW1 domain appears to be somewhat less stable than the WW2 domain, which is in agreement with our observation that the latter serves the role of a chaperonin for the former. In other words, the relative flexibility of the WW1 domain is likely to be important for its ligand binding function, while the relative stability of the WW2 domain is a manifestation of its ability to aid the function of the WW1 domain. Strikingly, the rather small fluctuations of atoms observed within the interdomain linker with respect to their counterparts within the constituent WW domains imply that their motions may be somewhat restricted relative to each other. This notion is indeed further supported through the assessment of the radius of gyration (R_g) of the WW1−WW2 tandem module as a function of simulation time (Figure 6c). It is evident from such analysis that the WW1−WW2 tandem module boasts a rather compact conformation, which undergoes rapid expansion as monitored by an increase in R_g during the first 50 ns burst phase. This is followed by a relaxation event that results in the WW1−WW2 tandem module becoming somewhat more compact in size than the starting conformation.

To investigate how a sharp increase followed by a rather slow decrease in R_g relates to conformational changes within the WW1−WW2 tandem module, we took structural snapshots of the protein at various time points during the course of our MD simulation (Figure 7). Consistent with our R_g analysis (Figure 6c), the constituent WW domains within the WW1−WW2

dx.doi.org/10.1021/bi400987k | Biochemistry 2013, 52, 9223−9236

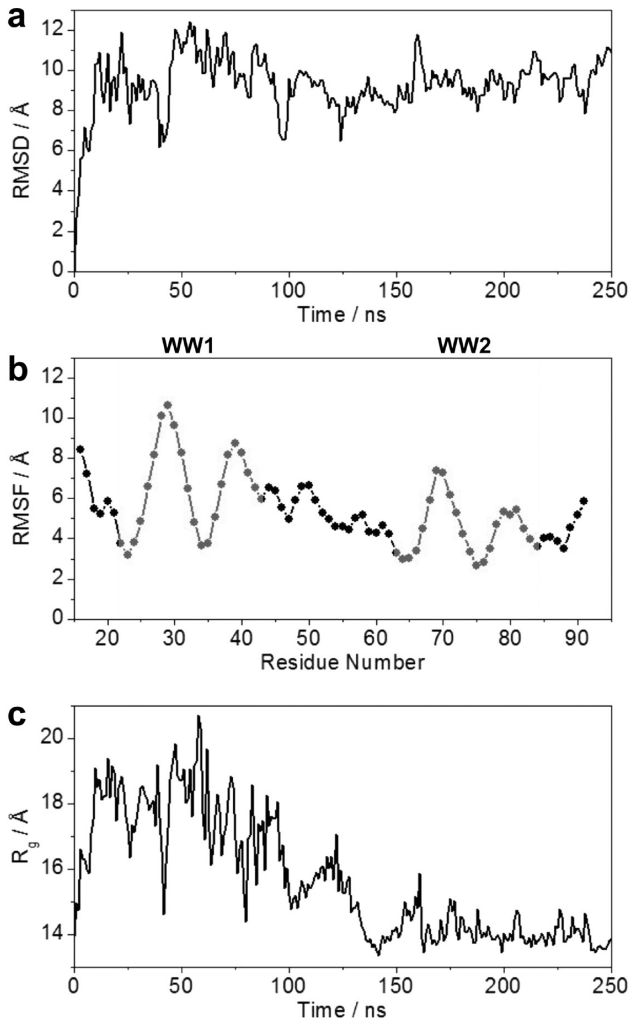

Figure 6. MD analysis conducted on the structural model of the WW1–WW2 tandem module of WWOX. (a) Root-mean-square deviation (rmsd) of backbone atoms (N, Cα, and C) within each simulated structure relative to the initial modeled structure as a function of simulation time. (b) Root-mean-square fluctuation (rmsf) of backbone atoms (N, Cα, and C) averaged over the entire course of the MD trajectory as a function of residue number. The vertical boxes demarcate the boundaries of WW1 and WW2 domains. (c) Radius of gyration (R_g) of each simulated structure relative to the initial modeled structure as a function of simulation time.

tandem module rapidly fall apart from their proximity observed in the starting conformation by virtue of the ability of the interdomain linker to uncoil. This relaxation step is slowly followed by compaction in which the two WW domains come together in a manner akin to physical association of two bodies. However, in light of the rather large rmsd observed for the WW1–WW2 tandem domain at structural equilibrium (Figure 6a), it is unlikely that such a compact conformation is stable and does not support their physical association in adopting a globular fold instead of a dumbbell-like conformation. Nonetheless, while the data presented above cannot ascertain the presence or absence of a stable physical association between the tandem WW domains of WWOX, their remarkable dynamic plasticity could in principle drive their transient physical association to allow the WW2 domain to chaperone the biological function of the WW1 domain.

CONCLUSIONS

Receptor tyrosine kinases (RTKs) play a key role in relaying extracellular signals in the form of growth factors, hormones, and cytokines to downstream effectors on the cytoplasmic side.[68−74] This information is then ultimately integrated via specific signaling cascades to regulate the transcriptional machinery within the nucleus in a wide variety of cellular processes central to human health and disease.[75−78] However, in recent years, it has increasingly become clear that RTKs such as ErbB4 may also employ an alternative mechanism for directly affecting gene transcription within the nucleus.[9,10,16] In this new paradigm of signal transduction,[11,12] the RTKs undergo proteolytic processing in response to mitogenic stimulation such that the cleaved fragment on the cytoplasmic side translocates to the nucleus and directly acts as a transcriptional regulator by virtue of its ability to collaborate with other cellular partners such as WWOX.

In an effort to understand the molecular basis of how such cleaved fragments affect gene transcription, we undertook the work presented here. With respect to this goal, our study shows that while the WW1 domain of WWOX binds to all three PPXY motifs (PY1–PY3) located within the ICD of ErbB4 in a highly promiscuous manner, the WW2 domain displays no ligand binding potential. Given that we have relied here on short peptides to mimic PPXY motifs in the ICD, caution is warranted in that these motifs may depart from their physiological behavior when they are treated as short peptides because of the loss of local conformational constraints to which they may be subjected in the context of the ICD. Additionally, the peptides used in our study were purposefully designed with charged amino and carboxyl termini to enhance their solubility in an aqueous buffer. While we recognize the fact that the protection of charged termini with amide and acetyl groups would have constituted better models of PPXY motifs, the loss of significant solubility of protected peptides clearly posed more technical challenges. We also note that the physiological relevance of PY1 and PY2 motifs in recruiting WWOX is questionable in light of the rather weak affinity with which they bind to the WW1 domain of WWOX compared to affinity of the PY3 motif. Interestingly, *in vivo* studies suggest that the interaction of WWOX with CYT1 and CYT2 isoforms of ErbB4 is indistinguishable.[18,21] Given the fact that CYT1 contains all three PPXY motifs (PY1–PY3) while CYT2 harbors only PY1 and PY3, the role of the PY2 motif does not appear to be important for driving the WWOX–ErbB4 interaction. On the other hand, while the binding of YAP to the PY3 motif has been demonstrated *in vivo*, binding to the PY1 motif was not observed.[16] We also note that Nedd4 ligases such as ITCH, WWP1, and NEDD4 have been suggested to exclusively bind to CYT1 but not CYT2 of ErbB4.[19,79−82] This finding thus invokes a unique role of the PY2 motif in driving the interaction of ErbB4 with members of the Nedd4 family.

On the basis of the data presented here, together with our previous work,[43] it appears increasingly likely that the WW2 domain is a putative orphan WW domain that is devoid of ligand binding capability and has evolved as a chaperone to augment the physiological function of the WW1 domain within WWOX. This notion is further corroborated by the observation that WWOX binds to its cellular partners exclusively through the WW1 domain.[18,22,37−39] Most importantly, we have also shown here that the ability of the WW2 domain to chaperone the WW1 domain within WWOX most likely lies in their

dx.doi.org/10.1021/bi400987k | *Biochemistry* 2013, 52, 9223−9236

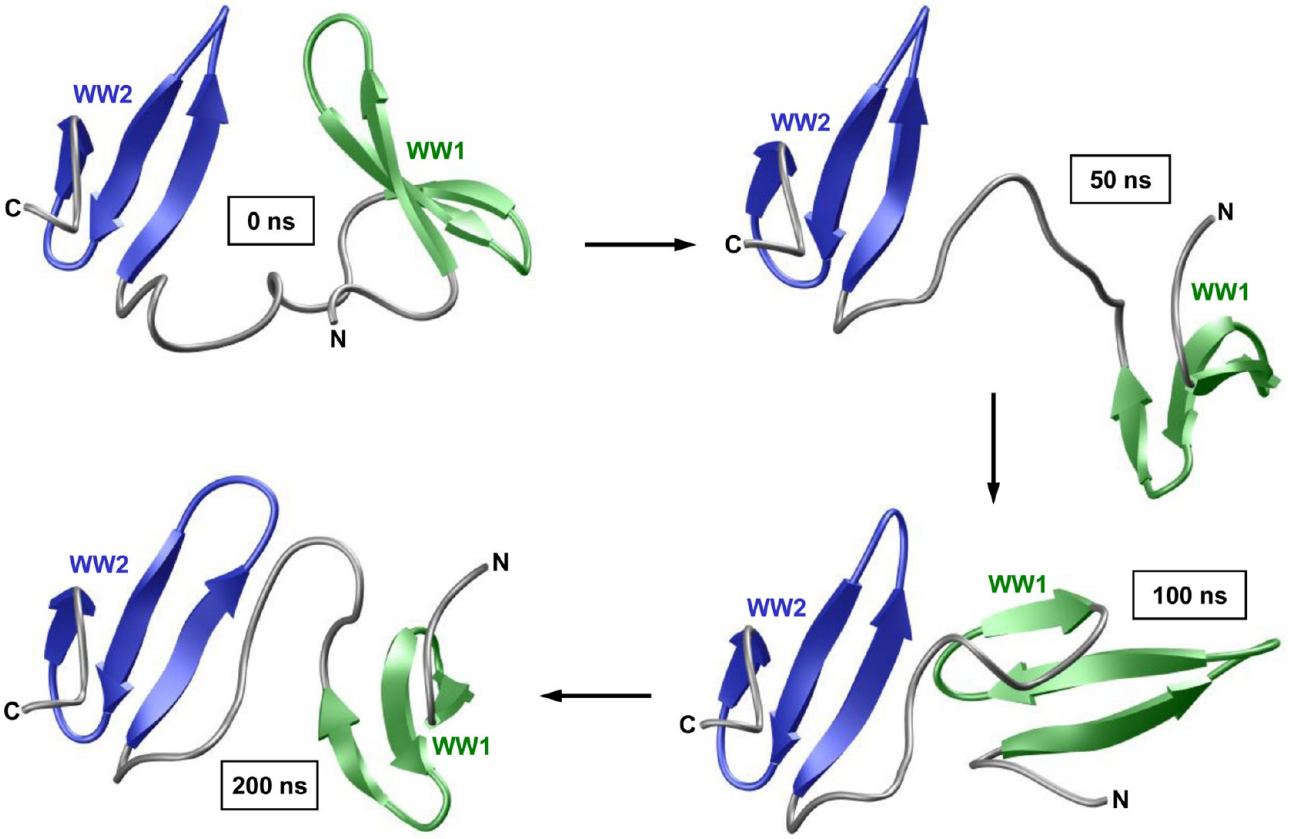

Figure 7. Structural snapshots taken at 0, 50, 100, and 200 ns during the course of an MD simulation conducted on the structural model of the WW1−WW2 tandem module of WWOX. The constituent WW1 and WW2 domains are colored green and blue, respectively, while the terminal and interdomain loops are colored gray for the sake of clarity.

dynamic plasticity that allows the WW2 domain to at least transiently associate with WW1. This scenario would be similar to that of the tandem WW domains of FBP21 pre-mRNA splicing factor[67] and the fruit fly suppressor of deltex Su(dx) involved in Notch signaling.[83] In both of these cases, the tandem WW domains are connected by a highly flexible loop, which allows them to move freely with respect to each other without a fixed orientation. On the other hand, stable physical association between the tandem WW domains of WWOX would likely impart rigidity and a fixed orientation upon them in a manner akin to that observed for the tandem WW domains of yeast splicing factor Prp40.[84] Notably, the interdomain linker in Prp40 is comprised of a well-ordered helix that appears to impart strict rigidity and a fixed orientation upon tandem WW domains. Accordingly, the tandem WW domains in Prp40 essentially act as a single rigid body, and the ligand binding grooves lie on opposite faces, which allows them to bind to distinct ligands and bridge precisely between target sites within the splicing machinery.

It is well-documented that the WW domains can be used to regulate cellular signaling pathways.[85,86] With respect to this goal, our demonstration that the WW2 domain of WWOX can be genetically manipulated through the Y85W substitution to generate the WW2W engineered domain that recognizes cognate ligands of the WW1 domain with high affinity bears therapeutic significance. In particular, the WW1−WW2W engineered tandem module could be therapeutically exploited to negatively regulate signaling pathways in response to hyperactivation of ErbB4 observed in a myriad of human disorders.[1−8] In short, our study offers not only molecular insights into the physical and thermodynamic forces at play in the operation of a key WW−ligand interaction involved in mediating a plethora of cellular processes but also new directions for the rational design of novel therapies with greater efficacy coupled with low toxicity for the treatment of human disease.

AUTHOR INFORMATION

Corresponding Author

*E-mail: amjad@farooqlab.net. Telephone: (305) 243-2429. Fax: (305) 243-3955.

Funding

This work was supported by National Institutes of Health Grant R01-GM083897 and funds from the USylvester Braman Family Breast Cancer Institute (to A.F.) and by Breast Cancer Coalition grants (RFA 50709 and RFA 60707) from the Department of Health of Pennsylvania (to M.S.). C.B.M. is a recipient of a postdoctoral fellowship from the National Institutes of Health (T32-CA119929).

Notes

The authors declare no competing financial interest.

ABBREVIATIONS

ALS, analytical light scattering; CD, circular dichroism; DLS, dynamic light scattering; ErbB4, erythroblastic (Erb) leukemia viral oncogene homologue B4; FBP21, formin binding protein 21; ITC, isothermal titration calorimetry; ITCH, ubiquitin ligase itchy homologue; LIC, ligation-independent cloning;

MM, molecular modeling; PPII, polyproline type II (helix); RTK, receptor tyrosine kinase; SEC, size-exclusion chromatography; SH3, Src homology 3; SLS, static light scattering; TPA, 12-*O*-tetradecanoyl phorbol 13-acetate; YAP, YES-associated protein; WWOX, WW domain-containing oxidoreductase.

REFERENCES

(1) Sundvall, M., Iljin, K., Kilpinen, S., Sara, H., Kallioniemi, O. P., and Elenius, K. (2008) Role of ErbB4 in breast cancer. *Journal of Mammary Gland Biology and Neoplasia 13*, 259−268.

(2) Sundvall, M., Veikkolainen, V., Kurppa, K., Salah, Z., Tvorogov, D., van Zoelen, E. J., Aqeilan, R., and Elenius, K. (2010) Cell death or survival promoted by alternative isoforms of ErbB4. *Mol. Biol. Cell 21*, 4275−4286.

(3) Veikkolainen, V., Vaparanta, K., Halkilahti, K., Iljin, K., Sundvall, M., and Elenius, K. (2011) Function of ERBB4 is determined by alternative splicing. *Cell Cycle 10*, 2647−2657.

(4) Hollmen, M., Liu, P., Kurppa, K., Wildiers, H., Reinvall, I., Vandorpe, T., Smeets, A., Deraedt, K., Vahlberg, T., Joensuu, H., Leahy, D. J., Schoffski, P., and Elenius, K. (2012) Proteolytic processing of ErbB4 in breast cancer. *PLoS One 7*, e39413.

(5) Paatero, I., Lassus, H., Junttila, T. T., Kaskinen, M., Butzow, R., and Elenius, K. (2013) CYT-1 isoform of ErbB4 is an independent prognostic factor in serous ovarian cancer and selectively promotes ovarian cancer cell growth in vitro. *Gynecol. Oncol. 129*, 179−187.

(6) Roskoski, R., Jr. (2004) The ErbB/HER receptor protein-tyrosine kinases and cancer. *Biochem. Biophys. Res. Commun. 319*, 1−11.

(7) Burgess, A. W. (2008) EGFR family: Structure physiology signalling and therapeutic targets. *Growth Factors 26*, 263−274.

(8) Wadugu, B., and Kuhn, B. (2012) The role of neuregulin/ErbB2/ErbB4 signaling in the heart with special focus on effects on cardiomyocyte proliferation. *Am. J. Physiol. 302*, H2139−H2147.

(9) Ni, C. Y., Murphy, M. P., Golde, T. E., and Carpenter, G. (2001) γ-Secretase cleavage and nuclear localization of ErbB-4 receptor tyrosine kinase. *Science 294*, 2179−2181.

(10) Lee, H. J., Jung, K. M., Huang, Y. Z., Bennett, L. B., Lee, J. S., Mei, L., and Kim, T. W. (2002) Presenilin-dependent γ-secretase-like intramembrane cleavage of ErbB4. *J. Biol. Chem. 277*, 6318−6323.

(11) Heldin, C. H., and Ericsson, J. (2001) Signal transduction. RIPping tyrosine kinase receptors apart. *Science 294*, 2111−2113.

(12) Ebinu, J. O., and Yankner, B. A. (2002) A RIP tide in neuronal signal transduction. *Neuron 34*, 499−502.

(13) Artavanis-Tsakonas, S., Rand, M. D., and Lake, R. J. (1999) Notch signaling: Cell fate control and signal integration in development. *Science 284*, 770−776.

(14) Fortini, M. E. (2002) γ-Secretase-mediated proteolysis in cell-surface-receptor signalling. *Nat. Rev. Mol. Cell Biol. 3*, 673−684.

(15) Cao, X., and Sudhof, T. C. (2001) A transcriptionally active complex of APP with Fe65 and histone acetyltransferase Tip60. *Science 293*, 115−120.

(16) Komuro, A., Nagai, M., Navin, N. E., and Sudol, M. (2003) WW domain-containing protein YAP associates with ErbB-4 and acts as a co-transcriptional activator for the carboxyl-terminal fragment of ErbB-4 that translocates to the nucleus. *J. Biol. Chem. 278*, 33334−33341.

(17) Omerovic, J., Puggioni, E. M., Napoletano, S., Visco, V., Fraioli, R., Frati, L., Gulino, A., and Alimandi, M. (2004) Ligand-regulated association of ErbB-4 to the transcriptional co-activator YAP65 controls transcription at the nuclear level. *Exp. Cell Res. 294*, 469−479.

(18) Aqeilan, R. I., Donati, V., Palamarchuk, A., Trapasso, F., Kaou, M., Pekarsky, Y., Sudol, M., and Croce, C. M. (2005) WW domain-containing proteins, WWOX and YAP, compete for interaction with ErbB-4 and modulate its transcriptional function. *Cancer Res. 65*, 6764−6772.

(19) Omerovic, J., Santangelo, L., Puggioni, E. M., Marrocco, J., Dall'Armi, C., Palumbo, C., Belleudi, F., Di Marcotullio, L., Frati, L., Torrisi, M. R., Cesareni, G., Gulino, A., and Alimandi, M. (2007) The E3 ligase Aip4/Itch ubiquitinates and targets ErbB-4 for degradation. *FASEB J. 21*, 2849−2862.

(20) Hoeing, K., Zscheppang, K., Mujahid, S., Murray, S., Volpe, M. V., Dammann, C. E., and Nielsen, H. C. (2011) Presenilin-1 processing of ErbB4 in fetal type II cells is necessary for control of fetal lung maturation. *Biochim. Biophys. Acta 1813*, 480−491.

(21) Aqeilan, R. I., Donati, V., Gaudio, E., Nicoloso, M. S., Sundvall, M., Korhonen, A., Lundin, J., Isola, J., Sudol, M., Joensuu, H., Croce, C. M., and Elenius, K. (2007) Association of Wwox with ErbB4 in breast cancer. *Cancer Res. 67*, 9330−9336.

(22) Del Mare, S., Salah, Z., and Aqeilan, R. I. (2009) WWOX: Its genomics, partners, and functions. *J. Cell. Biochem. 108*, 737−745.

(23) Bednarek, A. K., Laflin, K. J., Daniel, R. L., Liao, Q., Hawkins, K. A., and Aldaz, C. M. (2000) WWOX, a novel WW domain-containing protein mapping to human chromosome 16q23.3−24.1, a region frequently affected in breast cancer. *Cancer Res. 60*, 2140−2145.

(24) Bednarek, A. K., Keck-Waggoner, C. L., Daniel, R. L., Laflin, K. J., Bergsagel, P. L., Kiguchi, K., Brenner, A. J., and Aldaz, C. M. (2001) WWOX, the FRA16D gene, behaves as a suppressor of tumor growth. *Cancer Res. 61*, 8068−8073.

(25) Hezova, R., Ehrmann, J., and Kolar, Z. (2007) WWOX, a new potential tumor suppressor gene. *Biomedical Papers of the Medical Faculty of the University Palacký, Olomouc, Czechoslovakia 151*, 11−15.

(26) Nunez, M. I., Ludes-Meyers, J., Abba, M. C., Kil, H., Abbey, N. W., Page, R. E., Sahin, A., Klein-Szanto, A. J., and Aldaz, C. M. (2005) Frequent loss of WWOX expression in breast cancer: Correlation with estrogen receptor status. *Breast Cancer Res. Treat. 89*, 99−105.

(27) Aqeilan, R. I., Kuroki, T., Pekarsky, Y., Albagha, O., Trapasso, F., Baffa, R., Huebner, K., Edmonds, P., and Croce, C. M. (2004) Loss of WWOX expression in gastric carcinoma. *Clin. Cancer Res. 10*, 3053−3058.

(28) Aqeilan, R. I., and Croce, C. M. (2007) WWOX in biological control and tumorigenesis. *J. Cell. Physiol. 212*, 307−310.

(29) Aqeilan, R. I., Hagan, J. P., Aqeilan, H. A., Pichiorri, F., Fong, L. Y., and Croce, C. M. (2007) Inactivation of the Wwox gene accelerates forestomach tumor progression in vivo. *Cancer Res. 67*, 5606−5610.

(30) Pluciennik, E., Kusinska, R., Potemski, P., Kubiak, R., Kordek, R., and Bednarek, A. K. (2006) WWOX—the FRA16D cancer gene: Expression correlation with breast cancer progression and prognosis. *European Journal of Surgical Oncology 32*, 153−157.

(31) Lewandowska, U., Zelazowski, M., Seta, K., Byczewska, M., Pluciennik, E., and Bednarek, A. K. (2009) WWOX, the tumour suppressor gene affected in multiple cancers. *J. Physiol. Pharmacol. 60* (Suppl. 1), 47−56.

(32) Zelazowski, M. J., Pluciennik, E., Pasz-Walczak, G., Potemski, P., Kordek, R., and Bednarek, A. K. (2011) WWOX expression in colorectal cancer: A real-time quantitative RT-PCR study. *Tumor Biol. 32*, 551−560.

(33) Sudol, M., and Hunter, T. (2000) NeW wrinkles for an old domain. *Cell 103*, 1001−1004.

(34) Aqeilan, R. I., Trapasso, F., Hussain, S., Costinean, S., Marshall, D., Pekarsky, Y., Hagan, J. P., Zanesi, N., Kaou, M., Stein, G. S., Lian, J. B., and Croce, C. M. (2007) Targeted deletion of Wwox reveals a tumor suppressor function. *Proc. Natl. Acad. Sci. U.S.A. 104*, 3949−3954.

(35) Aqeilan, R. I., Hassan, M. Q., de Bruin, A., Hagan, J. P., Volinia, S., Palumbo, T., Hussain, S., Lee, S. H., Gaur, T., Stein, G. S., Lian, J. B., and Croce, C. M. (2008) The WWOX tumor suppressor is essential for postnatal survival and normal bone metabolism. *J. Biol. Chem. 283*, 21629−21639.

(36) Aqeilan, R. I., Hagan, J. P., de Bruin, A., Rawahneh, M., Salah, Z., Gaudio, E., Siddiqui, H., Volinia, S., Alder, H., Lian, J. B., Stein, G. S., and Croce, C. M. (2009) Targeted ablation of the WW domain-containing oxidoreductase tumor suppressor leads to impaired steroidogenesis. *Endocrinology 150*, 1530−1535.

(37) Aqeilan, R. I., Palamarchuk, A., Weigel, R. J., Herrero, J. J., Pekarsky, Y., and Croce, C. M. (2004) Physical and functional interactions between the Wwox tumor suppressor protein and the AP-2γ transcription factor. *Cancer Res. 64*, 8256−8261.

(38) Aqeilan, R. I., Pekarsky, Y., Herrero, J. J., Palamarchuk, A., Letofsky, J., Druck, T., Trapasso, F., Han, S. Y., Melino, G., Huebner,

K., and Croce, C. M. (2004) Functional association between Wwox tumor suppressor protein and p73, a p53 homolog. *Proc. Natl. Acad. Sci. U.S.A. 101*, 4401−4406.
(39) Ludes-Meyers, J. H., Kil, H., Bednarek, A. K., Drake, J., Bedford, M. T., and Aldaz, C. M. (2004) WWOX binds the specific proline-rich ligand PPXY: Identification of candidate interacting proteins. *Oncogene 23*, 5049−5055.
(40) Einbond, A., and Sudol, M. (1996) Towards prediction of cognate complexes between the WW domain and proline-rich ligands. *FEBS Lett. 384*, 1−8.
(41) Sudol, M. (1996) Structure and function of the WW domain. *Prog. Biophys. Mol. Biol. 65*, 113−132.
(42) Sudol, M. (2004) WW domain. In *Modular Protein Domains* (Cesareni, G. G., Sudol, M., and Yaffe, M., Eds.) pp 59−72, Wiley VCH, Verlag GmbH & Co., Weinheim, Germany.
(43) McDonald, C. B., Buffa, L., Bar-Mag, T., Salah, Z., Bhat, V., Mikles, D. C., Deegan, B. J., Seldeen, K. L., Malhotra, A., Sudol, M., Aqeilan, R. I., Nawaz, Z., and Farooq, A. (2012) Biophysical basis of the binding of WWOX tumor suppressor to WBP1 and WBP2 adaptors. *J. Mol. Biol. 422*, 58−74.
(44) Gao, X., Yo, P., Keith, A., Ragan, T. J., and Harris, T. K. (2003) Thermodynamically balanced inside-out (TBIO) PCR-based gene synthesis: A novel method of primer design for high-fidelity assembly of longer gene sequences. *Nucleic Acids Res. 31*, e143.
(45) Gasteiger, E., Hoogland, C., Gattiker, A., Duvaud, S., Wilkins, M. R., Appel, R. D., and Bairoch, A. (2005) Protein Identification and Analysis Tools on the ExPASy Server. In *The Proteomics Protocols Handbook* (Walker, J. M., Ed.) pp 571−607, Humana Press, Totowa, NJ.
(46) Wiseman, T., Williston, S., Brandts, J. F., and Lin, L. N. (1989) Rapid measurement of binding constants and heats of binding using a new titration calorimeter. *Anal. Biochem. 179*, 131−137.
(47) Zimm, B. H. (1948) The Scattering of Light and the Radial Distribution Function of High Polymer Solutions. *J. Chem. Phys. 16*, 1093−1099.
(48) Wyatt, P. J. (1993) Light Scattering and the Absolute Characterization of Macromolecules. *Anal. Chim. Acta 272*, 1−40.
(49) Berne, B. J., and Pecora, R. (1976) *Dynamic Light Scattering*, Wiley, New York.
(50) Chu, B. (1991) *Laser Light Scattering: Basic Principles and Practice*, Academic Press, Boston.
(51) Koppel, D. E. (1972) Analysis of Macromolecular Polydispersity in Intensity Correlation Spectroscopy. *J. Chem. Phys. 57*, 4814−4820.
(52) Marti-Renom, M. A., Stuart, A. C., Fiser, A., Sanchez, R., Melo, F., and Sali, A. (2000) Comparative Protein Structure Modeling of Genes and Genomes. *Annu. Rev. Biophys. Biomol. Struct. 29*, 291−325.
(53) Carson, M. (1991) Ribbons 2.0. *J. Appl. Crystallogr. 24*, 958−961.
(54) Van Der Spoel, D., Lindahl, E., Hess, B., Groenhof, G., Mark, A. E., and Berendsen, H. J. (2005) GROMACS: Fast, flexible, and free. *J. Comput. Chem. 26*, 1701−1718.
(55) Lindorff-Larsen, K., Piana, S., Palmo, K., Maragakis, P., Klepeis, J. L., Dror, R. O., and Shaw, D. E. (2010) Improved side-chain torsion potentials for the Amber ff99SB protein force field. *Proteins 78*, 1950−1958.
(56) Toukan, K., and Rahman, A. (1985) Molecular-dynamics study of atomic motions in water. *Phys. Rev. B 31*, 2643−2648.
(57) Darden, T. A., York, D., and Pedersen, L. (1993) Particle mesh Ewald: An N.log(N) method for Ewald sums in large systems. *J. Chem. Phys. 98*, 10089−10092.
(58) Hess, B., Bekker, H., Berendsen, H. J. C., and Fraaije, J. G. E. M. (1997) LINCS: A linear constraint solver for molecular simulations. *J. Comput. Chem. 18*, 1463−1472.
(59) Macias, M. J., Hyvonen, M., Baraldi, E., Schultz, J., Sudol, M., Saraste, M., and Oschkinat, H. (1996) Structure of the WW domain of a kinase-associated protein complexed with a proline-rich peptide. *Nature 382*, 646−649.
(60) Pires, J. R., Taha-Nejad, F., Toepert, F., Ast, T., Hoffmuller, U., Schneider-Mergener, J., Kuhne, R., Macias, M. J., and Oschkinat, H. (2001) Solution structures of the YAP65 WW domain and the variant L30 K in complex with the peptides GTPPPPYTVG, N-(n-octyl)-GPPPY and PLPPY and the application of peptide libraries reveal a minimal binding epitope. *J. Mol. Biol. 314*, 1147−1156.
(61) Huang, X., Poy, F., Zhang, R., Joachimiak, A., Sudol, M., and Eck, M. J. (2000) Structure of a WW domain containing fragment of dystrophin in complex with β-dystroglycan. *Nat. Struct. Biol. 7*, 634−638.
(62) Kanelis, V., Rotin, D., and Forman-Kay, J. D. (2001) Solution structure of a Nedd4 WW domain-ENaC peptide complex. *Nat. Struct. Biol. 8*, 407−412.
(63) Palencia, A., Camara-Artigas, A., Pisabarro, M. T., Martinez, J. C., and Luque, I. (2010) Role of interfacial water molecules in proline-rich ligand recognition by the Src homology 3 domain of Abl. *J. Biol. Chem. 285*, 2823−2833.
(64) Martin-Garcia, J. M., Ruiz-Sanz, J., and Luque, I. (2012) Interfacial water molecules in SH3 interactions: A revised paradigm for polyproline recognition. *Biochem. J. 442*, 443−451.
(65) Zafra-Ruano, A., and Luque, I. (2012) Interfacial water molecules in SH3 interactions: Getting the full picture on polyproline recognition by protein-protein interaction domains. *FEBS Lett. 586*, 2619−2630.
(66) Ohnishi, S., Guntert, P., Koshiba, S., Tomizawa, T., Akasaka, R., Tochio, N., Sato, M., Inoue, M., Harada, T., Watanabe, S., Tanaka, A., Shirouzu, M., Kigawa, T., and Yokoyama, S. (2007) Solution structure of an atypical WW domain in a novel β-clam-like dimeric form. *FEBS Lett. 581*, 462−468.
(67) Huang, X., Beullens, M., Zhang, J., Zhou, Y., Nicolaescu, E., Lesage, B., Hu, Q., Wu, J., Bollen, M., and Shi, Y. (2009) Structure and function of the two tandem WW domains of the pre-mRNA splicing factor FBP21 (formin-binding protein 21). *J. Biol. Chem. 284*, 25375−25387.
(68) Nimnual, A., and Bar-Sagi, D. (2002) The two hats of SOS. *Sci. STKE 2002*, PE36.
(69) Pierre, S., Bats, A. S., and Coumoul, X. (2011) Understanding SOS (Son of Sevenless). *Biochem. Pharmacol. 82*, 1049−1056.
(70) Li, N., Batzer, A., Daly, R., Yajnik, V., Skolnik, E., Chardin, P., Bar-Sagi, D., Margolis, B., and Schlessinger, J. (1993) Guanine-nucleotide-releasing factor hSos1 binds to Grb2 and links receptor tyrosine kinases to Ras signalling. *Nature 363*, 85−88.
(71) Rozakis-Adcock, M., Fernley, R., Wade, J., Pawson, T., and Bowtell, D. (1993) The SH2 and SH3 domains of mammalian Grb2 couple the EGF receptor to the Ras activator mSos1. *Nature 363*, 83−85.
(72) Chardin, P., Camonis, J. H., Gale, N. W., van Aelst, L., Schlessinger, J., Wigler, M. H., and Bar-Sagi, D. (1993) Human Sos1: A guanine nucleotide exchange factor for Ras that binds to GRB2. *Science 260*, 1338−1343.
(73) Nimnual, A. S., Yatsula, B. A., and Bar-Sagi, D. (1998) Coupling of Ras and Rac guanosine triphosphatases through the Ras exchanger Sos. *Science 279*, 560−563.
(74) Innocenti, M., Tenca, P., Frittoli, E., Faretta, M., Tocchetti, A., Di Fiore, P. P., and Scita, G. (2002) Mechanisms through which Sos-1 coordinates the activation of Ras and Rac. *J. Cell Biol. 156*, 125−136.
(75) Reuther, G. W., and Der, C. J. (2000) The Ras branch of small GTPases: Ras family members don't fall far from the tree. *Curr. Opin. Cell Biol. 12*, 157−165.
(76) Robinson, M. J., and Cobb, M. H. (1997) Mitogen-activated protein kinase pathways. *Curr. Opin. Cell Biol. 9*, 180−186.
(77) Hall, A. (1998) Rho GTPases and the actin cytoskeleton. *Science 279*, 509−514.
(78) Ridley, A. J. (2001) Rho GTPases and cell migration. *J. Cell Sci. 114*, 2713−2722.
(79) Sundvall, M., Korhonen, A., Paatero, I., Gaudio, E., Melino, G., Croce, C. M., Aqeilan, R. I., and Elenius, K. (2008) Isoform-specific monoubiquitination, endocytosis, and degradation of alternatively spliced ErbB4 isoforms. *Proc. Natl. Acad. Sci. U.S.A. 105*, 4162−4167.
(80) Li, Y., Zhou, Z., Alimandi, M., and Chen, C. (2009) WW domain containing E3 ubiquitin protein ligase 1 targets the full-length

ErbB4 for ubiquitin-mediated degradation in breast cancer. *Oncogene 28*, 2948−2958.
(81) Feng, S. M., Muraoka-Cook, R. S., Hunter, D., Sandahl, M. A., Caskey, L. S., Miyazawa, K., Atfi, A., and Earp, H. S., III (2009) The E3 ubiquitin ligase WWP1 selectively targets HER4 and its proteolytically derived signaling isoforms for degradation. *Mol. Cell. Biol. 29*, 892−906.
(82) Zeng, F., Xu, J., and Harris, R. C. (2009) Nedd4 mediates ErbB4 JM-a/CYT-1 ICD ubiquitination and degradation in MDCK II cells. *FASEB J. 23*, 1935−1945.
(83) Fedoroff, O. Y., Townson, S. A., Golovanov, A. P., Baron, M., and Avis, J. M. (2004) The Structure and Dynamics of Tandem WW Domains in a Negative Regulator of Notch Signaling, Suppressor of Deltex. *J. Biol. Chem. 279*, 34991−35000.
(84) Wiesner, S., Stier, G., Sattler, M., and Macias, M. J. (2002) Solution Structure and Ligad Recognition of the WW Domain of the Yeast Splicing Factor Prp40. *J. Mol. Biol. 324*, 807−822.
(85) Patnaik, A., and Wills, J. W. (2002) In vivo interference of Rous sarcoma virus budding by cis expression of a WW domain. *J. Virol. 76*, 2789−2795.
(86) Sudol, M., and Harvey, K. F. (2010) Modularity in the Hippo signaling pathway. *Trends Biochem. Sci. 35*, 627−633.